J Nanopart Res (2020) 22: 52
https://doi.org/10.1007/s11051-020-4777-x

RESEARCH PAPER

Carbon nanofiber based CuO nanorod counter electrode for enhanced solar cell performance and adsorptive photocatalytic activity

Bayram Kilic · Esra Bilgin Simsek · Sunay Turkdogan · Pelin Demircivi · Özlem Tuna · Selin Pravadili Mucur · Dusan Berek

Received: 17 May 2019 / Accepted: 10 February 2020 / Published online: 15 February 2020

Abstract Dye-sensitized solar cells (DSSCs) are known as new generation solar cell of photovoltaic technologies (PV), and have become hotspot topic in the PV research. DSSCs include four main components such as photoanode, counter electrode, dye, and electrolyte. The counter electrode is a vital component of DSSCs which has a significant effect on the solar cell performance and cost of the devices. In this research, CuO nanorod/carbon nanofiber (CuO/CNF) thin films are produced with the diameter of nanorods and vary from 10 to 50 nm as counter electrodes (CEs) for DSSCs. The applications of as-synthesized materials were also investigated in the field of photocatalysis. It was shown that CuO/CNF CE–based solar cells exhibited 6.5% solar cell efficiency (η) under solar irradiation. We demonstrate that CuO nanorods can be good alternatives for expensive platinum as it is composed of inexpensive and abundant materials and prepared by a simple fabrication process. CNF, exhibiting high carrier electron mobility, was employed to improve the catalytic and electrical properties of resulting CuO/CNF CEs. The power conversion efficiency of the DSSC was enhanced by almost 29% in the case of CuO/CNF CEs. In addition, the synthesized CuO/CNF nanoheterostructures exhibited superior photocatalytic activity toward the degradation of textile dye (Orange II) and antibiotic (tetracycline) compared to raw CuO. The enhanced efficiency can be ascribed to the reduction of E_g~band-gap energy and to the synergetic effect of adsorption and photocatalysis.

Keywords Carbon nanofiber · Copper oxide · Photocatalytic degradation · Dye-sensitized solar cell · Counter electrode · Nanostructured catalysts

B. Kilic (✉) · S. Turkdogan
Department of Energy Systems Engineering, Faculty of Engineering, Yalova University, 77100 Yalova, Turkey
e-mail: bkilic@yalova.edu.tr

e-mail: kbayramkilic@gmail.com

E. B. Simsek (✉) · P. Demircivi · Ö. Tuna
Department of Chemical and Process Engineering, Faculty of Engineering, Yalova University, 77100 Yalova, Turkey
e-mail: ebilgin.simsek@yalova.edu.tr

e-mail: esrabilgin622@gmail.com

S. P. Mucur
The Scientific and Technological Research Council of Turkey (TÜBİTAK) Marmara Research Center (MAM), Materials Institute, PK. 54, 41470 Gebze, Kocaeli, Turkey

D. Berek
Polymer Institute, Slovak Academy of Sciences, 84541 Bratislava, Slovakia

Introduction

In the last decades, the development of efficient, novel, and multifunctional materials has become an important issue to address many environmental and energy problems. Carbonaceous materials have gained much attention in both research and industry due to their high electrical conductivity, excellent catalyst support, large specific surface area, and high hydrogen adsorption

properties (Liang et al. 2018; Zeng et al. 2018). CNFs can be successfully used to form hybrid structures with different nanomaterials due to the aforementioned properties. Functionalization is another way to enhance unique properties of CNFs in the catalyst field and solar cells. One of the most essential ways to synthesize nanohybrids is to grow nanocrystals on the carbonaceous structure. After the nucleation step, chemical bonds between nanocrystals and carbon surface can be formed to promote a strong mechanical and electronic coupling within the hybrid structures (Darvishi et al. 2017). Carbon fiber–based photocatalysts possess a high performance for the degradation of organic pollutants due to their π-rich structure and high surface area. Some studies show that carbon fibers have been successfully decorated with different semiconductors including TiO_2 (Li et al. 2014; Oh et al. 2009; Wang et al. 2015), ZrO_2/TiO_2 (Bilgin Simsek et al. 2017), and cobalt (Wang et al. 2016). However, a literature review shows that the degradation processes using carbon fiber–based cupric oxide (CuO/CNF) photocatalysts have not yet been reported though CuO is a p-type semiconductor with high photochemical stability. CuO/CNF is composed of non-toxic and inexpensive materials, and it can be synthesized with a few simple and eco-friendly steps. CuO/CNF possesses narrow band-gap energy (~ 1.2–1.5 eV) with high light absorption efficiency, and this is why it has many potential applications in solar cells, photo-electrochemical cells, solid-state gas sensors, lithium-ion batteries, and photocatalysts (Langmar et al. 2015; Zhang et al. 2013). So far, CuO has been applied with different carbonaceous materials such as carbon nanotubes (Izaki et al. 2011; Qin et al. 2010), graphene oxide (Morandeira et al. 2008; Odobel and Pellegrin 2013), and activated carbon (Qin et al. 2010). A few studies about CuO deposited on carbon microfibers have been reported to increase the energy density of super-capacitors (Wood et al. 2014; Yu et al. 2012). The main purpose of this study is to grow CuO nanorods on the carbon fiber surface and to investigate the applications of resulting composite in the field of photocatalysis and dye-sensitized solar cells. CuO/CNF–based CEs were also investigated in DSSC applications, which have the advantages of relatively high-power conversion efficiency, low-cost, and simple fabrication, thus making them a potential competitor for conventional silicon-based solar cells (Liu et al. 2007; Nattestad et al. 2010). Typically, dye-sensitized solar cells (DSSCs) contain wide band-gap semiconductors such as TiO_2 or ZnO as photoanodes, having dye-coated photoanodes as solar light absorber, and electrolytes between photoanode and conventional platinum (Pt)-based counter electrodes (CEs), playing an important role of catalyzing iodide ions in redox reactions (Lepleux et al. 2009). However, Pt-based CEs are rather expensive, and therefore searching for alternatives has become a prominent effort to reduce their fabrication costs (Anandan et al. 2005). Selvaraj et al. (2018) show that the effect of transparent DSSCs on solar conversion efficiency indicated that the optoelectronic properties and devices performances of transparent DSSCs change the working electrode thicknesses. It has been shown that a very low concentrator with × 3 optical concentration was obtained and used to investigate the effect of light concentration on DSSCs (Selvaraj et al. 2018). Joshi et al. (2018) explained that the facile one-pot chemical reduction method for the synthesis of multiple-shaped AgNPs demonstrated its applicability for PCE enhancement in DSSCs. They indicated the fine tuning of SPR over 300–1000 nm by increasing the chemical reduction time and investigated their effect on the spectral response in DSSCs. High solar efficiency enhancement of ~ 30% has been obtained by using the composition of Mx-AgNPs in the photoactive material of DSSCs (Joshi et al. 2018). Joshi et al. (2018) studied the increase of solar conversion efficiency in DSSC, and in order to decrease the loss on photocurrent companion the electron-hole recombination, a simple method is developed in their work. They explain that the J_{sc} of the battery has been greatly improved after the treatment of the working electrode by a urea solution. At the concentration of an 1 g/ml urea solution, the highest devices efficiency was obtained, reaching 7.3%; compared with the pure P25 electrode, the efficiency of DSSC was increased by 25%. The enhancement of the efficiency is largely due to the C_3N_4 coating on the surface of photoanode, which is covered through very easy urea solution soak-calcination method and play the role of reducing the recombination of electrons (Joshi et al. 2018). Sarkar et al. (2018) explained the synthesis of a novel nanohybrid based on nickel sulfide (NiS) nanoparticles and decorated reduced graphene oxide (rGO) as a counter electrode in a steady state of a Pt-free counter electrode (CE) in DSSCs. The DSSC devices were obtained using this NiS/rGO nanohybrid film as CE demonstrate a high solar conversion efficiency of $\eta = 9.5\%$ (Sarkar et al. 2018).

In this study, CuO nanorods were deposited on CNF to investigate both the DSSCs' performance and photocatalytic activity. Here, we report a low-cost CE as a replacement of expensive platinum–FTO (Pt/F:SnO_2) CE to fabricate DSSCs. The influence of CuO/CNF on power conversion efficiency of DSSC was compared with a raw CuO employed as CE, and the results show that the efficiency increased from 5.06 to 6.50% due to the enhanced electron transport from CuO to CNF and eventually to the electrode. In addition, the photocatalytic decomposition was investigated for both orange textile dye and a selected antibiotic employing CuO/CNF composite, and the result shows that its performance was substantially higher compared to pure CuO. All the aforementioned results show that CuO/CNF heterostructures are very promising for the various catalytic applications.

Experimental method

Preparation of carbon fiber–based CuO nanorods

We prepare the microporous carbon fibers using a simple but versatile method as described in detail elsewhere (Simsek et al. 2017). Concisely, the microfibers of delignified cellulose were placed into a sealed stainless steel vessel and went through the carbonization process in an oven at 700 °C for an hour under CO_2, and released from cellulose in the first stage of carbonization. Carbon fibers formed by direct cellulose carbonization exhibit surface area in the range from 400 to 500 m^2g^{-1}. In order to prepare carbon fibers with higher surface areas, a $ZnCl_2$ porogen was employed. Delignified cellulose was under stirring, soaked with a solution of porogen, dried at 120 °C, and carbonized at 580 °C for 1 h. Next, the porogen was washed out with distilled water, and fibers were dried at 105 °C. The concentration of $ZnCl_2$ porogen in cellulose subject to carbonization was 15, 30, or 50 wt% correspondingly; the carbon fibers with surface areas 802, 1365, and 2270 m^2g^{-1} were obtained. They are denoted CNF1, CNF2, and CNF3, respectively.

The dip-coating method was utilized to deposit CNFs on the FTO substrate. Copper oxide nanorods were grown over the CNF-coated FTO substrate by the hydrothermal method. A solution of 100 mg $CuCl_2 + 2H_2O$ in 40 mL of distilled water was prepared and poured into a Teflon-lined stainless steel autoclave. In order to adjust the overall solution's PH level to 9, 2 ml of ammonia (28%) was slowly added (Kilic, 2019). After adjusting its PH level, we dipped CNF/FTO substrates into the solution and followed by heating to 190 °C for 24 h. After the hydrothermal growth process, the entire system was allowed to cool naturally to room temperature, and the substrate was dried under N_2 flow. Finally, the CuO film was deposited on the CNF/FTO substrate, and the sample was put into a furnace at 350 °C followed by the annealing for 30 min to minimize the defect states. The final products were named as CuO/CNF1, CuO/CNF2, and CuO/CNF3.

Study of photocatalytic degradation

Orange II and tetracycline (TC) were picked as model pollutants to examine the photocatalytic activity of the composite catalysts. Visible light irradiation experiments were conducted in a photoreactor, provided with two halogen visible light sources. Photocatalytic degradation of Orange II in water solution (10 mg L^{-1}) and tetracycline solutions (20 mg L^{-1}) was studied. A catalyst of 0.01 g was transferred into 50 mL of pollutant solution. In order to get the adsorption–desorption equilibrium, the solution was stirred for 30 min in the absence of light. Samples (4 mL) were regularly collected at different time intervals, and their concentrations were determined by the UV-Visible spectrophotometer at 485 nm and 360 nm, respectively. Photocatalytic activities of the composites CuO/CNF1, CuO/CNF2, and CuO/CNF3 were investigated under different reaction conditions. Initial pollutant concentrations were 10, 20, or 30 mg L^{-1}; pH of their solution was adjusted to 3, 6 or 10; and catalyst dosage was 0.05, 0.1, or 0.2 g L^{-1}.

Device fabrication of DSSCs based on CNF/CuO nanorod counter electrodes

A photoanode based on nano semiconductor materials was prepared on a FTO substrate by the hydrothermal method as explained in detail elsewhere (Kilic et al. 2017). In order to prepare the photoanode side of a DSSC, N719 dye materials were adsorbed on the photoanode's surface by dipping the substrate into the N719 solution for 12 h. It is noteworthy that the photoanode was put into the oven at 90 °C for 40 min before absorption of the N719 dye solution. The dye-sensitized photoanode and CuO/CNF CE were sandwiched with a transparent film, and I^-/I^{3-} was used

as the liquid electrode. J–V data was gathered employing a Keithley 175A digital multimeter with 0.01-V intervals per second under a AM 1.5 solar simulator. A 250-W tungsten halogen lamp with solar filter was arranged to irradiate the samples at 100 mW/cm^2.

Results and discussion

Structural and optical characterizations

The surface morphology of CuO nanorods, grown on a carbon fiber substrate, is seen in Fig. 1a–c. As seen in Fig. 1a, pure CNF can be grown on a FTO substrate with high surface area and homogeneous distribution. Figure 1 b shows urchin-like CuO nanorods that can be obtained at about a 50-nm diameter on FTO. Figure 1 c indicated that CuO/CNF nanostructures have been uniformly grown on the substrate by the hydrothermal method. It shows that the CuO nanorods are well coated on CNF-based substrate and make a good contact with CNF, which is very important for a good electrical conductivity. The diameter of nanorods varies from 10 to 50 nm, and their length reaches 2 μm. XRD results in Fig. 1d show that the material has diffraction peaks at 33.73°, 39.92°, and 49.42°, corresponding to CuO (110), (200), and (− 202) planes, respectively. The average crystal size of the nanostructures, calculated from Scherrer's formula by taking CuO (200) plane into account, was in the range of 10–20 nm. Figure 1 e shows EDX measurements of CNF/CuO hybrid structures. We confirm that CuO nanostructures have grown on CNF structures.

XPS measurements were carried out to explain the surface chemical state and chemical compositions of elements in CNF-based CuO nanostructures (Fig. 2a–e). Photoelectron peaks for Cu, O, and C elements were recorded as in Fig. 2a with a wide scan. Figure 2 b shows the Cu 2p spectra of Cu $2p_{1/2}$ and $2p_{3/2}$ located at 952.8 eV and 932.9 eV, confirming the presence of copper elements. As obviously seen in Fig. 2c, O 1s shows two main peaks at about 532.6 eV and 530.8 eV, indicating the adsorption oxygen (O_{ads}) and the lattice oxygen, respectively. It suggests two kinds of links, namely the CuO bonds and the surface-adsorbed carbonate anions. Figure 2 d shows three main XPS peaks of C 1s at about 284.3 eV, 286.2 eV, and 288.9 eV.

UV-Vis measurements were utilized to reveal the optical properties of CuO and CuO/CNF/2 nanostructures. Figure 3 a–d show absorption measurements of the samples. The spectrums show that CuO absorbs light in the entire visible region of the spectrum. E_g~band-gap energy of the nanostructures was calculated by using well-known Tauc plots and were produced using the absorption spectra (Anandan et al. 2005; Kilic et al. 2017; Simsek et al. 2017). Band-gap energies of CuO and CuO/CNF/2 nanostructures were indicated from intercepts of the extrapolated linear region of the Tauc plots with the "hv" axis. As seen in Fig. 3b–d, pure CuO and CuO/CNF/2 composites have the band-gap energy values of 1.56 eV and 1.29 eV, respectively, and those values are matching with the literature data (Kilic et al. 2017; Wang et al. 2001). It was shown that Cu incorporation into CNF might be the reason of decreased band-gap energy.

Photocatalytic activity measurements

Preliminary adsorption and photodegradation studies

Adsorption kinetics of CuO and CuO/CNF/2 catalysts were investigated in dark with the catalyst dosage of 0.2 g/L. Figure 4 presents the dynamic curves for the adsorption of Orange II and tetracycline over the catalysts. For the raw CuO sample, the Orange II adsorption balance was established within 30 min, and no significant change was observed in the degradation between 60 and 180 min. On the other hand, the Orange II adsorption reached saturation with CuO/CNF/2 catalyst after 120 min of treatment. At the end of 3 h, Orange II adsorptive removal efficiencies of CuO and CuO/CNF/2 catalysts were calculated as 17.9% and 51.5%, respectively. The higher removal of CuO/CNF/2 catalysts could be ascribed to the strong π–π interactions of carbon fiber surface and dye molecules (Prabhakarrao et al. 2017). Similar phenomenon was also observed for TC adsorption. At the end of the 120-min period, the TC removal performance was calculated as 50.3% and 55.8% for CuO and CuO/CNF/2 catalysts, respectively.

The photocatalytic activities of CuO and CuO/CNF/2 were assessed by the degradation of Orange II and TC under visible light irradiation. The CuO/CNF/2 catalyst showed superior catalytic performance towards the dye and antibiotic molecules when compared with raw CuO. Results show that the degree of photodegradation of Orange II

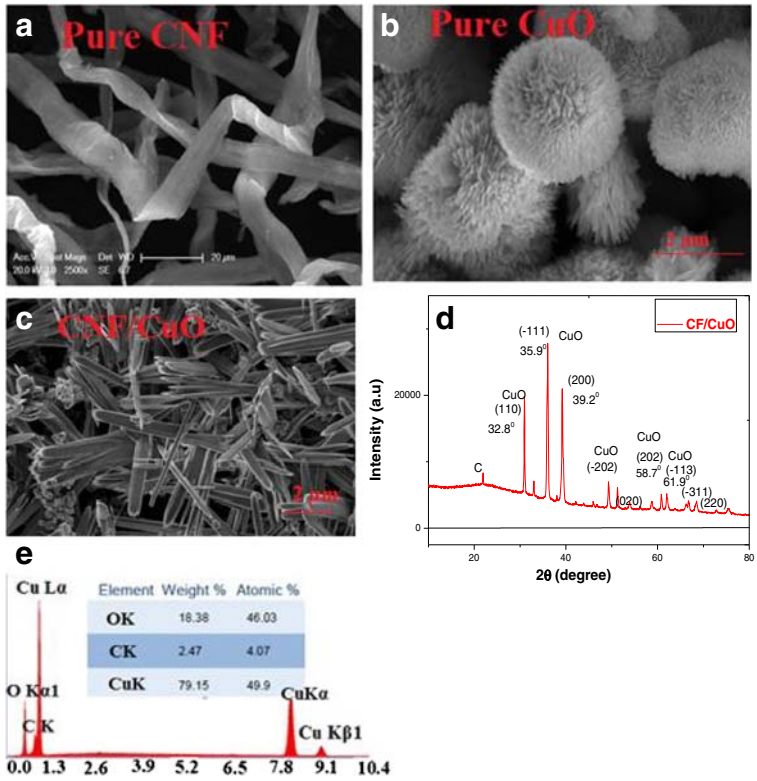

Fig. 1 **a–c** SEM images of CuO/CNF nanostructures with different magnification, **d** XRD characterization of CuO/CNF

achieved in 4 h was 86.1% and 21.2% by CuO/CNF/2 and CuO catalysts, respectively. Similarly, after 4 h of visible light irradiation, about 81.2% and 74.8% of TC was decomposed by CuO/CNF/2 and

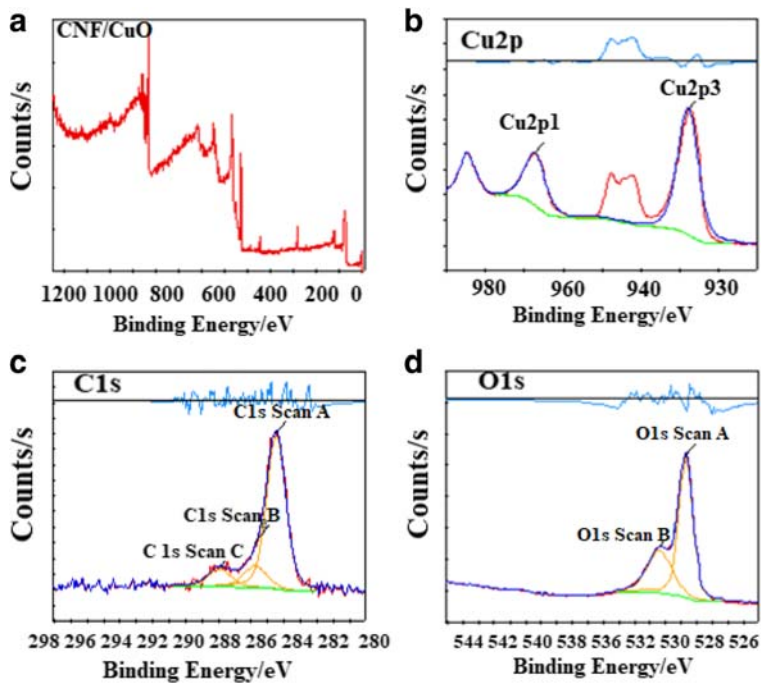

Fig. 2 **a–d** XPS spectra of CuO/CNF nanostructures: (**a**) wide scan range of CNF/CuO, (**b**) narrow scan of Cu 2p level peak, (**c**) C1s level peak, (**d**) O 1s level peak

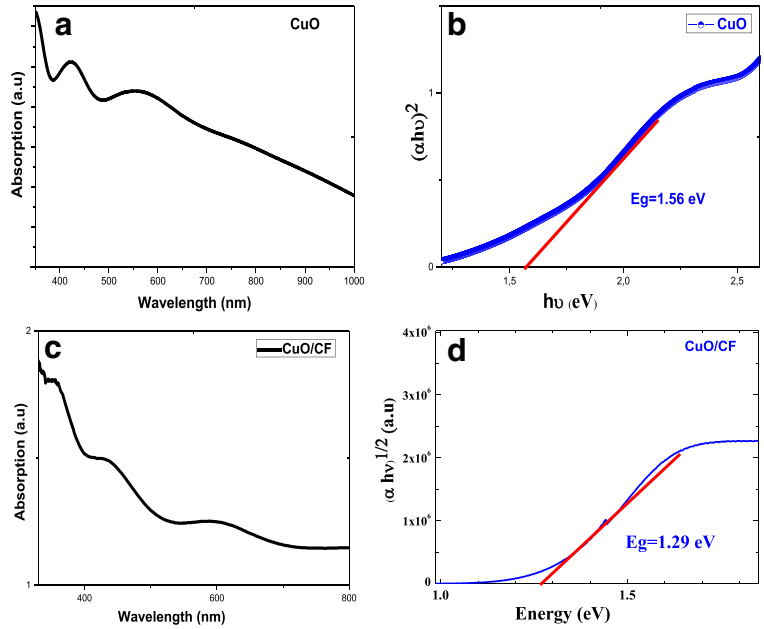

Fig. 3 **a–b** Absorbance spectra and absorption coefficient/energy plots for films of CuO. **c–d** Absorbance spectra and absorption coefficient/energy plots for films of CuO/CNF

CuO catalysts, respectively. The rate of decomposition was depended on the catalyst type. The CuO/CNF/2 heterostructure catalyst was found to be more effective most likely due to the dual effect of photolysis and adsorption (Oh et al. 2009; Wang et al. 2015).

The *Langmuir–Hinshlwood* kinetic model was used to describe the photocatalytic performance of the pure CuO and the composites CuO/CNF/2. The model is expressed as $\ln(C_0/C) = k_{app}.t$, where $k_{app}(min^{-1})$ is the constant apparent rate, and C and C_0 are the concentrations at the time "t" and "at the beginning of the degradation," respectively. The k_{app} values increased when CNF was incorporated into the CuO nanorods structure. The rate constants were determined as $2.90 \times 10^{-2}$and 3.67×10^{-2} min^{-1} for TC degradation, whereas they were 2.13×10^{-2} and 2.82×10^{-2} min^{-1} for Orange II degradation when CuO and CuO/CNF/2 photocatalysts were used, respectively.

Effect of carbon nanofiber surface area

In order to examine the effect of carbon fiber surface area, the photocatalytic experiments were performed with CuO/CNF(1), CuO/CNF(2), and CuO/CNF(3) catalysts under visible light irradiation, and the results are presented in Fig. 4. The photocatalytic degradation rates of Orange II dye and TC are obviously influenced by different surface area of CNF in the CuO/CNF heterostructures. The Orange II dye photodegradation efficiency was obtained as 18% for CuO/CNF/1, while the efficiency as high as 95% was observed for CuO/CNF/3 catalyst. In case of CuO/CNF/1 and CuO/CNF/2, the antibiotic degradation was found to be 79.7% and 81.2%, respectively, and subsequently enhanced to 88.7% for the CuO/CNF/3 catalyst. It is anticipated that in the catalysts with higher surface area, a larger number of accessible active sites promote high photocatalytic activity (Panneri et al. 2017; Wang et al. 2001). Considering the photocatalytic efficiency and economy, the CuO/CNF/2 sample was chosen as an optimum catalyst for further experiments.

Regarding the mechanism of photocatalysis, the catalytic efficiency of CuO/CNF heterostructure could be influenced by multiple effects: absorption of light which ends up producing electrons and holes, carrier separation with interfacial electron transfer, adsorption of molecules, and reaction between photogenerated electrons/holes and the molecules. The most effective step is the formation of photogenerated electrons and holes where the active holes occur by reaction the holes in the valence band with the active groups of the catalyst surface. Furthermore, the recombination of the active parts can be inhibited in order to prevent decrease in the catalytic performance. Therefore, we can conclude that the surface and electronic properties of carbonaceous catalysts are significantly important for the catalytic performance.

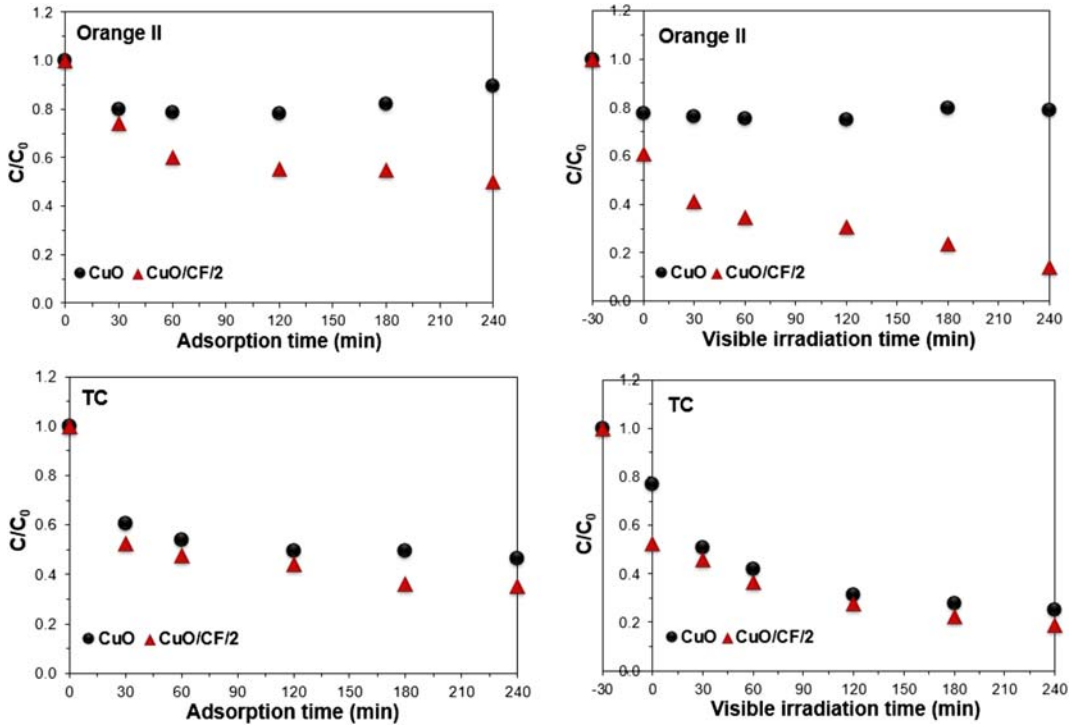

Fig. 4 Dark adsorption kinetics and photodegradation under visible light irradiation

Effect of pH

The influence of pH on the Orange II and TC degradation activity was studied at different initial pH values. As presented in Fig. 5, the degradation percentage of Orange II got a maximum (92%) at pH 3, and it decreased with increasing pH, from pH 6.7 (84%) to pH 10 (70%). Since the azo-dye molecules have two pK_a values (10.6 and 1), Orange II molecules could assume different forms at different pH values: (i) doubly protonated (H_2L) at pH lower than 1, (ii) mono protonated (HL^-) in the pH range between 1 and 10.6, and (iii) nonprotonated (L^{2-}) at pH higher than 10.6 (Abramian and El-Rassy 2009). In addition, the catalyst surface is positively charged under acidic conditions, while it is negatively charged in alkaline media. Therefore, the protonation significantly affects the Orange II adsorption via electrostatic forces at acidic pHs.

On the other hand, the TC photodegradation reached maximum at pH 6.2 (88% degradation), while it was reduced to 77% at pH 3.0. The molecular structure of TC and surface functional groups of CNF plays an important role in adsorptive photocatalysis by CuO/CNF. TC molecules exhibit three acidity constants: the

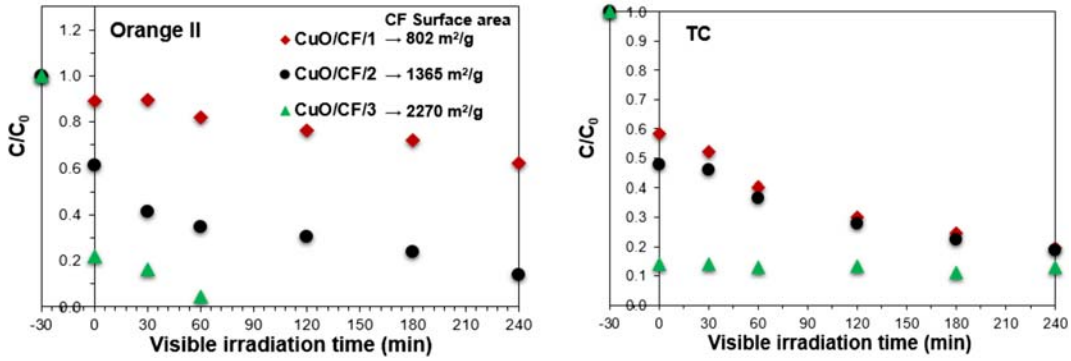

Fig. 5 Effect of carbon fiber surface area on the photocatalytic performance of Orange II and TC

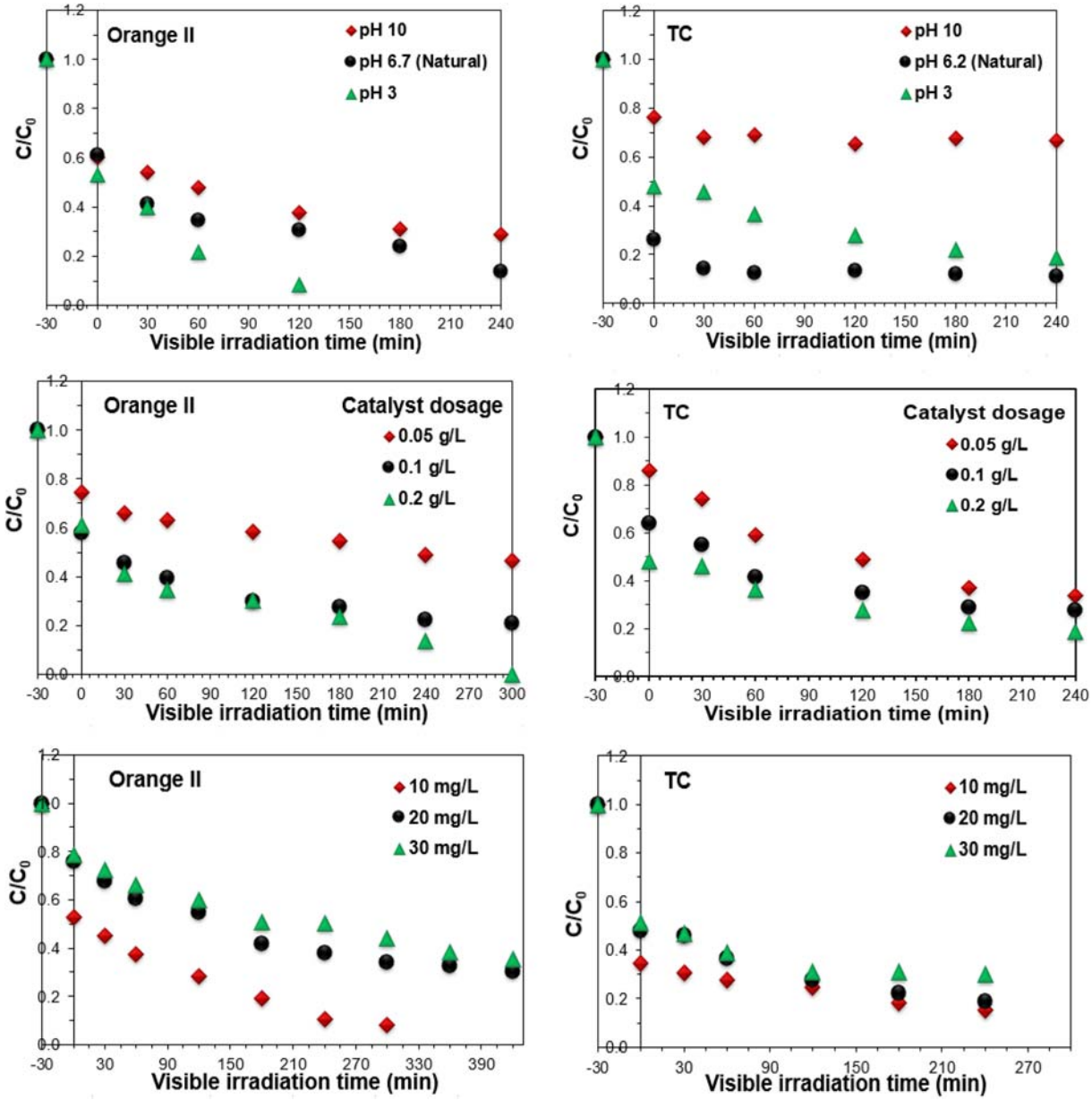

Fig. 6 Effect of (**a**) pH (**b**) catalyst dosage (**c**) initial solution concentration on the photocatalytic degradation by CuO/CNF catalyst

first deprotonation (H_3TC^+, $pK_{a1} = 3.3$); the second pK value (H_2TC^0, $pK_{a2} = 7.7$); and the third one (HTC^-, TC^{2-} $pK_{a3} = 9.7$) is attributed to the protonated nitrogen of the dimethylamino groups (Chen et al. 2011). Under acidic conditions, the TC molecules are positively charged, while they exist as zwitterionic and anionic species under neutral and alkaline media, respectively. At pH 3.0, the electrostatic repulsion occurs between cationic forms of TC and positively charged CuO/CNF/2. In the pH range from 3.0 to 6.2, $H_2TC°$ species are adsorbed onto the positive charged CuO/CNF/2 surface ($pH_{IEP} = 6.7$). The electrostatic attraction/repulsion forces are not the main driving force in the TC adsorption by carbonaceous materials (Li et al. 2018). The adsorption can occur via non-electrostatic π–π interactions among the catalyst surface, benzene rings and double bonds (C=C, C=O) of the tetracycline, or via hydrophobic interactions (Wang et al. 2018). When pH is above 7.7 (pK_{a2}), the electrostatic repulsion occurs between the predominant HTC^- and TC^{2-} species and

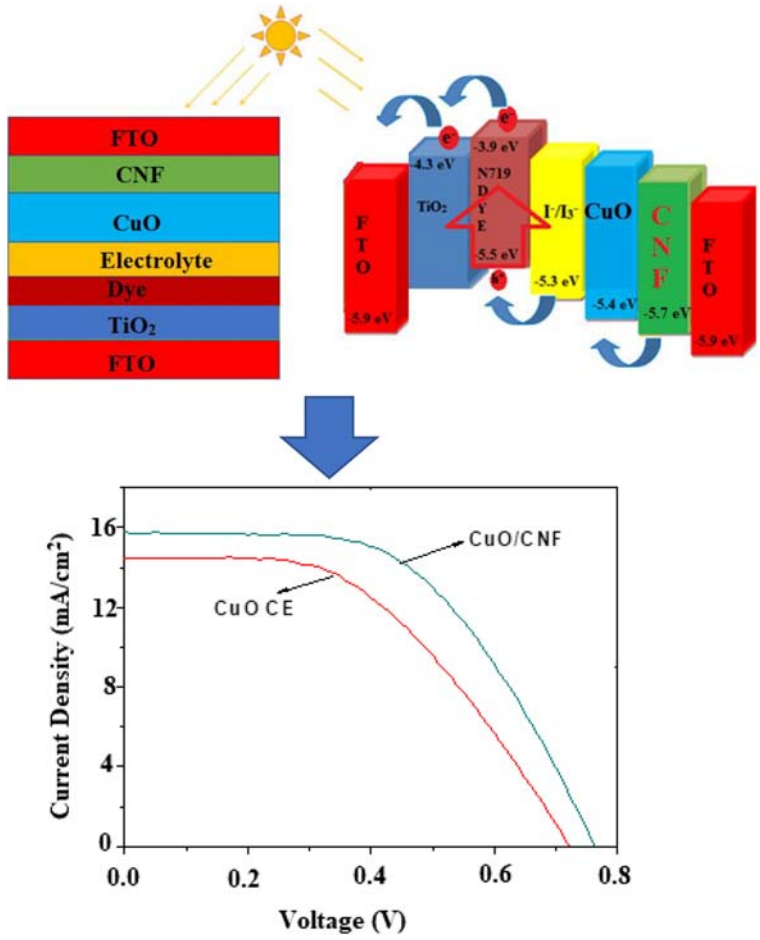

Fig. 7 **a** Current-voltage (I–V) characteristics of CuO/CNF-based dye-sensitized solar cells under 1-Sun AM 1.5G solar irradiance

negatively charged surface of CuO/CNF/2. Hence, the photodegradation efficiency decreased to 32% at pH 10.

Effect of initial pollutant concentration

Since the photocatalytic activity depends on the initial concentration of pollutant, the experiments were performed with constant catalytic dosage (10 mg), by altering the concentration of dye from 10 to 30 ppm under visible irradiation, as illustrated in Fig. 6. The photocatalytic degradation of dye and antibiotic molecules decreased with the increase of initial concentration. When the initial Orange II concentration was 30 mg/L, the lowest degradation percentage (50%) was obtained, while it was observed as 85% for the initial concentration of 10 mg/L. The decrease in the degradation rate is related with the number of •OH/•O_2^- radicals formed on the catalyst surface, while the number of active sites keeps stable at a constant catalyst dosage. Hence, increasing of the concentration of dye/antibiotic species may block the active sites for •OH generation. Moreover, the adsorbed dye/antibiotic molecules on the catalyst surface may reduce the radiation path length in light intensity for photocatalyst excitation (Ajmal et al. 2016).

Table 1 Photovoltaic properties of DSSCs based on CuO and CNF/CuO nanostructures

Sample	FF (%)	(%)	V_{oc}	I_{sc}	P_{max}
CuO	48.6	5.06	0.72	14.48	1.26
CNF/CuO	54.44	6.50	0.76	15.72	1.62

Effect of catalyst dosage

The effect of catalyst dosage in the range of 0.05–0.2 g/L was evaluated by the photodegradation experiments,

and the results are illustrated in Fig. 6. The degradation efficiency of Orange II was 46% and 85% at the doses of 0.05 g/L and 0.2 g/L, respectively. Similarly, the TC degradation level increased from 72 to 77% when catalyst doses were increased from 0.1 to 0.2 g/L after 180 min of visible irradiation. The increase can be explained by the formation of more active sites within catalyst, which is responsible for both the cleavage of the dye molecules and increased dye adsorption. At the same time, the increase in catalyst dosage raises the number of photogenerated sites, which are responsible for faster dye degradation.

Devices characterization

Schematic illustration and J–V curves of CuO and CuO/CNF/2 CEs-based DSSCs are illustrated in Fig. 7. Photovoltaic parameters such as J_{sc}, V_{oc}, FF, and η of each cell are summarized in Table 1. Compared with a pure CuO counter electrode, the CuO/CNF/2 counter electrode makes the solar cell deliver 28.7% more power. The DSSCs with CuO/CNF/2 CE exhibited a J_{sc} of 15.72 (mA/cm^2), V_{oc} of 0.76 V, FF of 54%, and η of 6.50%. The improvement of solar cell efficiency is mainly the due to increased J_{SC}, which can be attributed to rapid inter conversion between I_3^- and I^-, possible reflection of incident photons from CNF/CuO CE, and low band-gap of hybrid structures. Since CNF/CuO has a band-gap energy of 1.29 eV, photons can be absorbed in the interface, and generated electrons in conduction band may contribute the J_{SC} of DSSC through the transport process either to electrolyte or working electrode. We indicated that CNF/CuO CE can also provide a large effective surface area owing to their rough morphology, leading to low charge transfer resistance. Since CuO/CNF/2 has a low band-gap energy of 1.29 eV, photons in a wide wavelength range can be absorbed in nano-surface and generate electron-hole pairs contributing to I_{SC} of DSSC. In addition to those, CuO/CNF/2 CE possesses highly surface area due to their rough morphology, which leads to a low charge transfer resistance.

Conclusions

CuO/CNF nanostructure–based counter electrodes in DSSCs were studied, and results indicated a substantial improvement in the cell efficiency compared to the conventional Pt counter electrode. It was also confirmed that CuO/CNF thin films have a larger surface area, and thus showing a better catalytic activity than the conventional Pt CE. Because of the aforementioned reasons, the cell exhibited the higher solar conversion efficiency of 6.50%. Based on the above results, CuO/CNF-based CEs show a great potential to be used in DSSCs' industry to promote the cell efficiency with a versatile and low-cost growth method. Carbon fiber–based CuO nanorod catalysts also showed excellent adsorptive photocatalytic degradation under visible light illumination and high solar conversion efficiency in DSSCs as CE. It was also shown that when the band-gap gets narrower, and thus red-shifting the absorption edge, the e^-/h^+ separation toward the photodegradation of dye and antibiotic pollutants are improved.

Acknowledgments The authors would like to thank Ivan Novak from Slovak Academy of Sciences, Slovakia for help on the carbon fiber synthesis.

Compliance with ethical standards

Conflict of interest The authors declare that they have no competing interests.

References

Abramian L, El-Rassy H (2009) Adsorption kinetics and thermodynamics of azo-dye Orange II onto highly porous titania aerogel. Chem Eng J 150:403–410

Ajmal A et al (2016) Photocatalytic degradation of textile dyes on Cu2O-CuO/TiO2 anatase powders. J Environ Chem Eng 4: 2138–2146. https://doi.org/10.1016/j.jece.2016.03.041

Anandan S, Wen X, Yang S (2005) Room temperature growth of CuO nanorod arrays on copper and their application as a cathode in dye-sensitized solar cells. Mater Chem Phys 93: 35–40

Bilgin Simsek E, Demircivi P, Berek D, Novák I (2017) Fabrication of carbon fiber supported zirconium–titanium nanocomposites for efficient photocatalytic decolorization of Orange II dye under visible light irradiation. React Kinet Mech Catal:124. https://doi.org/10.1007/s11144-017-1320-x

Chen H, Luo H, Lan Y, Dong T, Hu B, Wang Y (2011) Removal of tetracycline from aqueous solutions using polyvinylpyrrolidone (PVP-K30) modified nanoscale zero valent iron. J Hazard Mater 192:44–53

Darvishi M, Mohseni-Asgerani G, Seyed-Yazdi J (2017) Simple microwave irradiation procedure for the synthesis of CuO/Graphene hybrid composite with significant photocatalytic enhancement. Surfaces and Interfaces 7:69–73

Izaki M et al (2011) Electrodeposition of 1.4-eV-bandgap p-copper (II) oxide film with excellent photoactivity. J Electrochem Soc 158:D578–D584

Joshi DN, Ilaiyaraja P, Sudakar C, Prasath RA (2018) Facile one-pot synthesis of multi-shaped silver nanoparticles with tunable ultra-broadband absorption for efficient light harvesting in dye-sensitized solar cells. Sol Energy Mater Sol Cells 185: 104–110

Kilic B, Turkdogan S, Astam A, Baran SS, Asgin M, Cebeci H, Urk D (2017) Graphene-based copper oxide thin film nanostructures as high-efficiency photocathode for p-type dye-sensitized solar cells. J Photonics for Energy 7:045502

Kılıç B (2019) Interface effect of graphene–TiO_2 photoanode with CuO nanorod counter electrode on solar conversion efficiency and enhanced external quantum efficiency. Opt Quant Electron 51(6):208

Langmar O, Ganivet CR, Lennert A, Costa RD, De La Torre G, Torres T, Guldi DM (2015) Combining electron-accepting phthalocyanines and nanorod-like CuO electrodes for p-type dye-sensitized solar cells. Angew Chem Int Ed 54: 7688–7692

Lepleux L, Chavillon B, Pellegrin Y, Blart E, Cario L, Jobic S, Odobel F (2009) Simple and reproducible procedure to prepare self-nanostructured NiO films for the fabrication of p-type dye-sensitized solar cells. Inorg Chem 48:8245–8250

Li M-f et al (2018) Performance of magnetic graphene oxide/diethylenetriaminepentaacetic acid nanocomposite for the tetracycline and ciprofloxacin adsorption in single and binary systems. J Colloid Interface Sci 521:150–159

Li Y, Liu C, Xu P, Li M, Zen M, Tang S (2014) Controlled fabrication of ordered mesoporous titania/carbon fiber composites with high photoactivity: synergistic relationship between surface adsorption and photocatalysis. Chem Eng J 243:108–116

Liang Y et al (2018) Enhanced dye photocatalysis and recycling abilities of semi-wrapped TiO2@ carbon nanofibers formed via foaming agent driving. Ceram Int 44:1711–1718

Liu Y, Liao L, Li J, Pan C (2007) From copper nanocrystalline to CuO nanoneedle array: synthesis, growth mechanism, and properties. J Phys Chem C 111:5050–5056

Morandeira A, Boschloo G, Hagfeldt A, Hammarstrom L (2008) Coumarin 343− NiO films as nanostructured photocathodes in dye-sensitized solar cells: ultrafast electron transfer, effect of the I3−/I− redox couple and mechanism of photocurrent generation. J Phys Chem C 112:9530–9537

Nattestad A, Mozer AJ, Fischer MK, Cheng Y-B, Mishra A, Bäuerle P, Bach U (2010) Highly efficient photocathodes for dye-sensitized tandem solar cells. Nat Mater 9:31

Odobel F, Pellegrin Y (2013) Recent advances in the sensitization of wide-band-gap nanostructured p-type semiconductors. Photovoltaic and photocatalytic applications. J Phys Chem Lett 4:2551–2564

Oh W-C, Zhang F-J, Chen M-L, Lee Y-M, Ko W-B (2009) Characterization and relative photonic efficiencies of a new Fe-ACF/TiO2 composite photocatalysts designed for organic dye decomposition. J Ind Eng Chem 15:190–195

Panneri S, Ganguly P, Mohan M, Nair BN, Mohamed AAP, Warrier KG, Hareesh U (2017) Photoregenerable, bifunctional granules of carbon-doped g-C3N4 as adsorptive photocatalyst for the efficient removal of tetracycline antibiotic. ACS Sustain Chem Eng 5:1610–1618

Prabhakarrao N, Chandra MR, Rao TS (2017) Synthesis of Zr doped TiO2/reduced Graphene Oxide (rGO) nanocomposite material for efficient photocatalytic degradation of Eosin Blue dye under visible light irradiation. J Alloys Compd 694:596–606

Qin P et al (2010) Synthesis and mechanistic studies of organic chromophores with different energy levels for p-type dye-sensitized solar cells. J Phys Chem C 114:4738–4748

Sarkar A, Chakraborty AK, Bera S (2018) NiS/rGO nanohybrid: an excellent counter electrode for dye sensitized solar cell. Sol Energy Mater Sol Cells 182:314–320

Selvaraj P et al (2018) Enhancing the efficiency of transparent dye-sensitized solar cells using concentrated light. Sol Energy Mater Sol Cells 175:29–34

Simsek EB, Novak I, Sausa O, Berek D (2017) Microporous carbon fibers prepared from cellulose as efficient sorbents for removal of chlorinated phenols. Res Chem Intermed 43: 503–522

Wang J, Liu R, Yin X (2018) Adsorptive removal of tetracycline on graphene oxide loaded with titanium dioxide composites and photocatalytic regeneration of the adsorbents. J Chem Eng Data 63:409–416

Wang T, Li Y, Qu G, Liang D, Hu S (2016) Photocatalytic degradation of acid orange II using activated carbon fiber-supported cobalt phthalocyanine coupled with hydrogen peroxide. Water Air Soil Pollut 227:464

Wang W, Zhan Y, Wang G (2001) One-step, solid-state reaction to the synthesis of copper oxide nanorods in the presence of a suitable surfactant. Chem Commun:727–728

Wang Z, Yoshinaga K, Bu XR, Zhang M (2015) Low temperature fabrication & photocatalytical activity of carbon fiber-supported TiO2 with different phase compositions. J Hazard Mater 290:134–141

Wood CJ et al (2014) Red-absorbing cationic acceptor dyes for photocathodes in tandem solar cells. J Phys Chem C 118: 16536–16546

Yu M, Natu G, Ji Z, Wu Y (2012) p-type dye-sensitized solar cells based on delafossite CuGaO2 nanoplates with saturation photovoltages exceeding 460 mV. J Phys Chem Lett 3: 1074–1078

Zeng Z, Chen S, Tan TTY, Xiao F-X (2018) Graphene quantum dots (GQDs) and its derivatives for multifarious photocatalysis and photoelectrocatalysis. Catal Today 315: 171–183

Zhang Z, Dua R, Zhang L, Zhu H, Zhang H, Wang P (2013) Carbon-layer-protected cuprous oxide nanowire arrays for efficient water reduction. ACS Nano 7:1709–1717